THE JOURNAL OF PHYSICAL CHEMISTRY C
A JOURNAL OF THE AMERICAN CHEMICAL SOCIETY

pubs.acs.org/JPCC

Article

Topological Crystalline Insulator Phases in Magnetic van der Waals Crystal $MnBi_4Te_7$ and $Mn_2Bi_2Te_5$ Families

Jia-Yi Lin,[#] Zhipeng Cao,[#] Zhong-Jia Chen, Wenxin He, Jiarui Zeng, Xiao-Bao Yang, Yichen Hua, Ji-Hai Liao, and Yu-Jun Zhao*

Cite This: *J. Phys. Chem. C* 2024, 128, 20451−20458

Read Online

ACCESS | Metrics & More | Article Recommendations | Supporting Information

ABSTRACT: In the past several years, the discoveries of multiple magnetic topological phases in $MnBi_2Te_4$ and its analogues have highlighted the research in modern condensed matter physics. The topological crystalline insulator (TCI) phase protected by space group symmetry is a valuable platform to understand the profound relation of crystalline symmetry and band topology in materials. Via first-principles calculations, we predict that the $MnBi_2Te_4$ analogues, $MnBi_4Te_7$, $MnSb_4Te_7$, $Mn_2Bi_2Te_5$, and $Eu_2Bi_2Te_5$, are all mirror-symmetry-protected TCI candidates when magnetized along the in-plane x orientation. Gapless surface states are expected for the van der Waals terminations in this phase. Particularly, the magnetic easy axis of $Eu_2Bi_2Te_5$ is along the in-plane direction in our calculations. These findings open opportunities for research and application of magnetic TCIs and magnetically controllable topological quantum phase transitions.

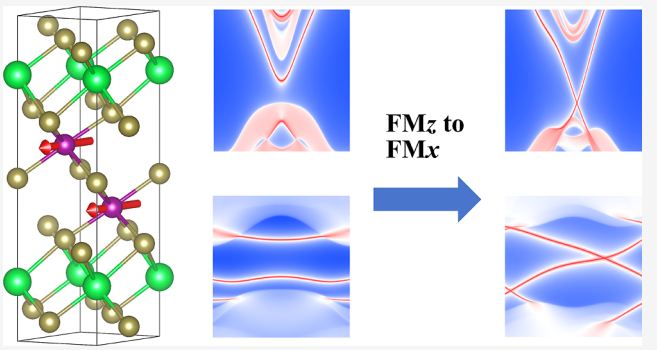

INTRODUCTION

As one of the most fantastic subjects in modern condensed matter physics, topological quantum physics has attracted enormous research interest and efforts.[1] Since the early concept model was conceived, a series of topological quantum states in condensed matter have been predicted theoretically and realized experimentally.[2,3] The exotic dissipationless quantum transport phenomena, such as the quantum spin Hall effect and the quantum anomalous Hall effect, were discovered in topological materials.[4] Meanwhile, the quasiparticle dispersions in condensed matter, such as Dirac Fermion, Weyl Fermion, and Majorana Fermion, are predicted to exist on these platforms. These advances shed light on the basic theoretical physics research and future applications of quantum computation, quantum materials, and devices.[5,6]

In the early days, the discovery of topological quantum materials was most in the nonmagnetic platforms, establishing the earliest topological material database.[7−9] In 2022, Vergniory et al. screened all topological bands of all nonmagnetic stoichiometric materials in the Inorganic Crystal Structure Database (ICSD).[10] It seems that the discovery of topological quantum electronic states in nonmagnetic materials is now well-established. In addition to the topological electronic states, the database of topological phonon states in materials has also been established by Xu et al. very recently.[11]

Unlike the nonmagnetic counterparts, the research of magnetic topological quantum states is still hindered by a lack of sufficient material realizations since the theoretical calculation for magnetic materials is more complicated than that for nonmagnetic materials. However, there are advantages of magnetic topological materials that their nonmagnetic counterparts cannot achieve. For example, the topological phases of magnetic systems are always strongly coupled with the magnetic configurations since these configurations determine the magnetic space group symmetry. Consequently, multiple magnetic topological phases and magnetically controllable topological quantum phase transitions are expected in these systems, offering opportunities for tunable spintronics device applications.

The earliest concept model of the antiferromagnetic (AFM) topological insulator (TI) was conceived in 2010.[12] However, the first AFM TI phase in condensed matter was not discovered until 2019, when $MnBi_2Te_4$ was unveiled.[13] Subsequently, the AFM axion insulator (AXI) phase and ferromagnetic (FM) Weyl semimetal phase were discovered in $MnBi_2Te_4$.[14] Furthermore, it was pointed out that the number of layers significantly influences the topological phases and magnetic coupling of $MnBi_2Te_4$ thin films.[15] The quantum anomalous Hall effect was also discovered in this material

Received: August 30, 2024
Revised: November 6, 2024
Accepted: November 7, 2024
Published: November 13, 2024

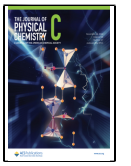

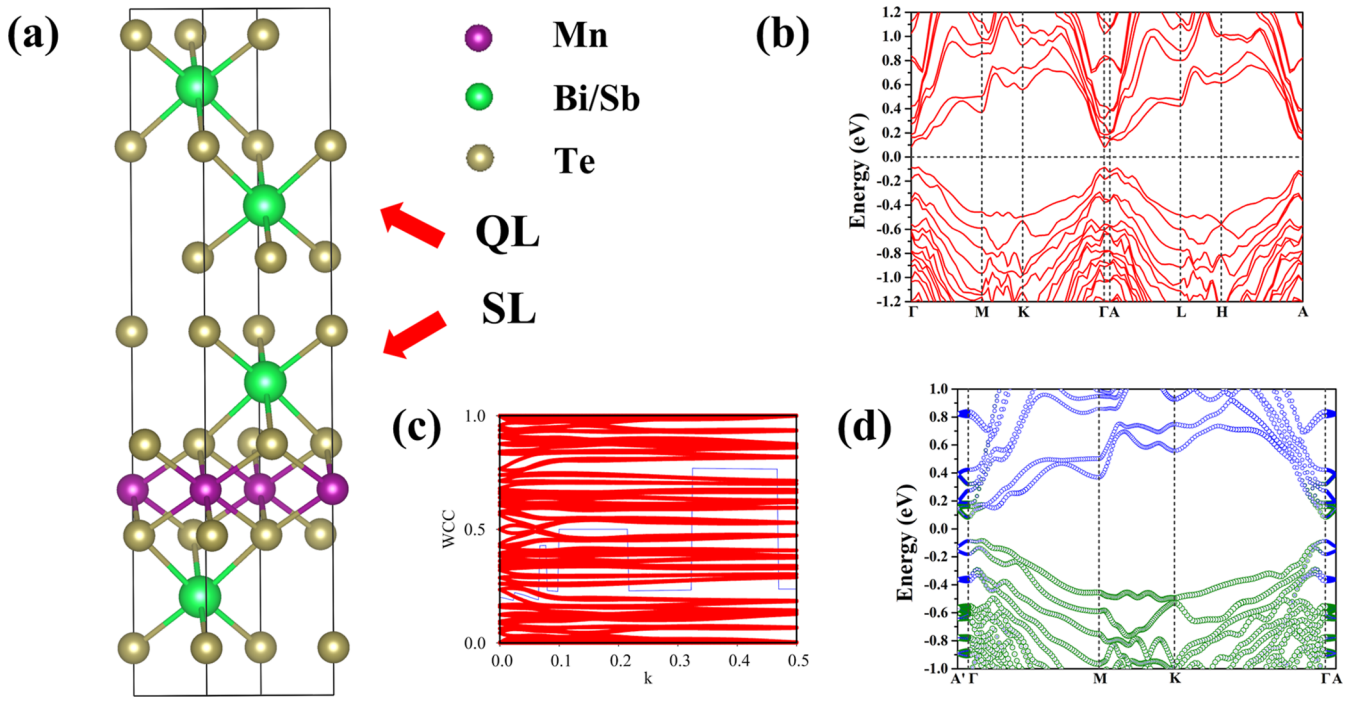

Figure 1. Crystal and electronic structures of $MnBi_4Te_7$. (a) Crystal structure of $MnBi_4Te_7$ or $MnSb_4Te_7$, (b) bulk band structure of $MnBi_4Te_7$ in the A-AFM*x* configuration, (c) WCC of $MnBi_4Te_7$ in the A-AFM*x* configuration, and (d) projected inverted band of $MnBi_4Te_7$ in the A-AFM*x* configuration, in which the blue bubbles represent the Bi p orbital projection and the olive bubbles represent the Te p orbital projection.

platform.[16] Similar quantum phenomena were also predicted or realized in $MnSb_2Te_4$ and $MnBi_2Se_4$ under certain conditions.[17−19] Recently, the second-order topological corner states in $MnBi_2Te_4$ films were predicted by Zhan et al.[20] The coexistence of superconductivity and antiferromagnetism was also discovered in $MnBi_2Te_4$.[21] Novel magnetic exchange bias effects, magnetic transport, and photon electronic properties were also discovered in this material family.[22−27]

Unlike the previous TIs protected by time-reversal symmetry, topological crystalline insulators (TCIs) represent another class of topological materials protected by certain space group symmetries.[28] Band degeneracy would appear on certain high-symmetry crystal surfaces in TCIs, which is important for understanding the profound relationship between the band topology and the crystalline space group or magnetic space group symmetries. Similar to the case of TIs, TCI materials were also first discovered in the nonmagnetic systems.[29] In the case of $MnBi_2Te_4$, Li et al. predicted that it is a TCI protected by mirror symmetry in the A-type antiferromagnetic (A-AFM) with spins aligned along the *x* axis.[30] Although this TCI phase is not easily realized in experiments since the magnetic easy axis of $MnBi_2Te_4$ is along the out-of-plane direction and a slight external magnetic field may turn the system into an FM configuration due to the weak interlayer magnetic coupling in this van der Waals (vdW) material, it demonstrates that TCI phases may widely exist in this material family and its analogues. In our previous work, we predicted that such a TCI phase also emerges in $MnBi_4Se_7$ and $MnSb_4Se_7$ in the FM*x* magnetic configuration.[31]

In this work, we predict that a series of well-known AFM TIs, including $MnBi_4Te_7$, $MnSb_4Te_7$, $Mn_2Bi_2Te_5$, and $Eu_2Bi_2Te_5$, are TCIs when magnetized along the in-plane *x* orientation as determined by first-principles calculations. These TCI phases are protected by the $x = 0$ mirror symmetry, and thus, gapless surface states are expected to emerge on the (001) vdW termination surface, which facilitates experimental observation of these topological quantum states. Notably, the predicted easy axis of $Eu_2Bi_2Te_5$ is along the in-plane direction. These findings will open opportunities for future research and applications in the field of magnetic topological physics and magnetically controllable topological quantum phase transitions.

METHODS

All the calculations in this work were conducted using density functional theory (DFT) via the Vienna ab initio simulation package (VASP).[32−34] The computations were performed within generalized gradient approximation (GGA), with Perdew−Burke−Ernzerhof (PBE) functional for the exchange−correlation potential except the MAE test of $Eu_2Bi_2Te_5$.[35] The projector-augmented wave (PAW) approach was employed.[36,37] To expand the Kohn−Sham wave functions, we set an energy cutoff of 405 eV for the plane wave basis set.[38] The criterion for energy convergence of the electronic self-consistent field (SCF) was set to 1×10^{-8} eV/cell. The coordinations of all atoms were fully relaxed until the forces were smaller than $1 \times 1 \times 10^{-4}$ eV/Å. The spin−orbit coupling (SOC) effect is included in all calculations. To appropriately include the strong correlation of Mn 3d and Eu 4f electrons, we employed the DFT + *U* method with *U*(Mn 3d) = 5.34 eV and *U*(Eu 4f) = 7 eV.[39,40] The *U* value of Mn 3d was reported to yield a similar band gap to the HSE06 functional in A-AFM*z* $MnBi_2Te_4$, and it is widely used in a series of analogous materials. The *U* value of Eu 4f is the same as in Wang et al.'s work. To include the van der Waals interactions, the DFT-D4 method is used.[41] $18 \times 18 \times 6$ Γ-centered *k*-mesh is set for the SCF calculations. We calculated the band representations and magnetic topological SIs using irvsp, TopMat, and Mvasp2trace codes.[42,43] We constructed

https://doi.org/10.1021/acs.jpcc.4c05870
J. Phys. Chem. C 2024, 128, 20451−20458

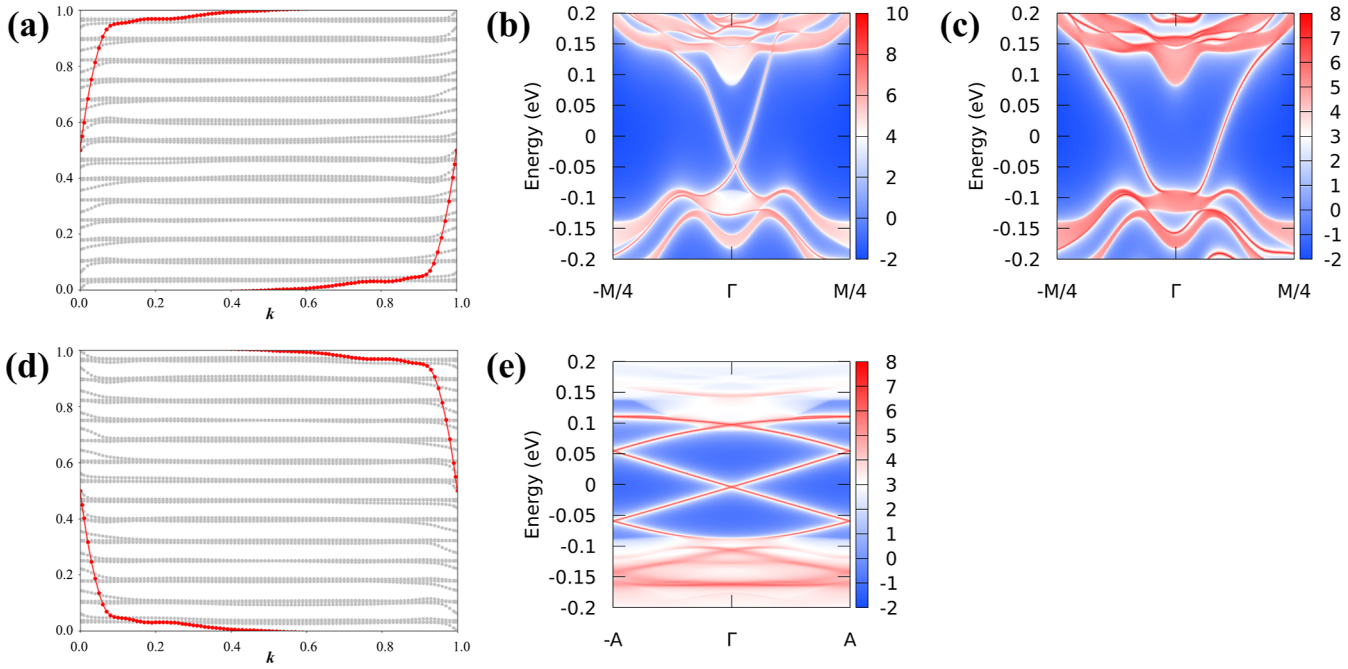

Figure 2. MCNs and surface LDOS of $MnBi_4Te_7$ in the A-AFMx configuration. (a) WCC of the $m_x = +i$ subspace, (b) (001) surface LDOS on QL termination, (c) (001) surface LDOS on SL termination, (d) WCC of the $m_x = -i$ subspace, and (e) (010) surface LDOS.

the Wannier Hamiltonians by using Wannier90 codes.[44−46] To construct the Wannier Hamiltonians, Mn 4s, Mn 3d, Bi 6p, Sb 5p, Te 5p, and Eu 4f orbitals are included for the projections. Specifically, 78, 66, and 70 projectors are employed for Mn(Bi, Sb)$_4$Te$_7$, $Mn_2Bi_2Te_5$, and $Eu_2Bi_2Te_5$ per primitive cell, respectively. To obtain well-localized Wannier functions, we set 2000 steps for the disentanglement procedure and required at least 256 input DFT bands per primitive cell. To maintain the symmetry of the Wannier Hamiltonians, we adopt a zero step of the wannierization procedure. The Wilson loop and surface-state local density of states (LDOS) were calculated by the WannierTools package.[47]

RESULTS AND DISCUSSION

The crystal structures of $MnBi_4Te_7$, $MnSb_4Te_7$, $Mn_2Bi_2Te_5$, and $Eu_2Bi_2Te_5$ are of the $P\bar{3}m1$ (no. 164) space group. In the paramagnetic configuration, their magnetic space group is $P\bar{3}m11'$ (no. 164.86) with the group operators written as follows

$$G = \{\hat{E}, \hat{P}, \hat{C}_{3z}, \hat{M}_x\} \otimes \{\hat{E}, \hat{T}\} \tag{1}$$

where $\hat{E}$ stands for the identity operator, $\hat{P}$ for the parity operator, $\hat{C}_{3z}$ for the 3-fold rotation around the z axis, $\hat{M}_x$ for the mirror operator about the $x = 0$ plane, and $\hat{T}$ for the time-reversal operator. When the spins align along the out-of-plane direction, namely, the z axis, the $\hat{C}_{3z}$ symmetry is preserved but the $\hat{M}_x$ symmetry is broken down. However, when the spins align along the x orientation, the mirror symmetry $\hat{M}_x$ survived as the $\hat{C}_{3z}$ symmetry is broken. In the ferromagnetic (FMx) configuration, the magnetic space group is of $C2/m$ (no. 12.58), with the operators written as follows

$$G = \{\hat{E}, \hat{P}, \hat{M}_x\} \tag{2}$$

In the A-AFMx configuration, the magnetic space group is of C_c2/m (no. 12.63), with the symmetry operators written as follows

$$G = S \cup \{\hat{T}|\tau_{1/2}\}S \tag{3}$$

where

$$S = \{\hat{E}, \hat{P}, \hat{M}_x\} \tag{4}$$

Thus, when the magnetization orientation is along the x axis, a mirror-symmetry-protected TCI phase is possible since $\hat{M}_x$ survived according to eqs 1−4, which offers opportunities for the magnetically controllable topological quantum phase transition.

As shown in Figure 1a, the crystal structure of Mn(Bi, Sb)$_4$Te$_7$ consists of a Mn(Bi, Sb)$_4$Te$_7$ septuple layer (SL) and (Bi, Sb)$_2$Te$_3$ quintuple layer (QL), stacking along the z direction via vdW interaction.[48,49] Using the PBE-D4 + U method,[50] we obtain the bulk band structure of $MnBi_4Te_7$ in the A-AFMx configuration, as shown in Figure 1b. The calculated bulk band gap is a 166.6 meV direct band gap at the Γ point. In this magnetic configuration, the bulk bands are all double degenerate, guaranteed by the $\hat{P}$ and $\hat{T}\tau_{1/2}$ symmetries. Since these two symmetry operations are preserved, the $\mathbb{Z}_2$ topological invariant can be calculated to diagnose the band topology by the following formula

$$(-1)^{\lambda} = \prod_{k_{\mathrm{inv}}, n\in \mathrm{occ}/2} \xi_n(k_{\mathrm{inv}}) \tag{5}$$

where k_{inv} is the time-reversal invariant k points in the first Brillouin zone, n runs over all the occupied Kramers' pairs, and λ is the $\mathbb{Z}_2$ topological invariant.[51,52] In our calculation, topologically nontrivial $\mathbb{Z}_2 = 1$ is obtained by eq 5 in this A-AFMx configuration. Thus, $MnBi_4Te_7$ is an AFM TI in the A-AFMx state, which is the same as the A-AFMz magnetic ground state. We also calculated the flow of Wannier charge

https://doi.org/10.1021/acs.jpcc.4c05870
J. Phys. Chem. C 2024, 128, 20451−20458

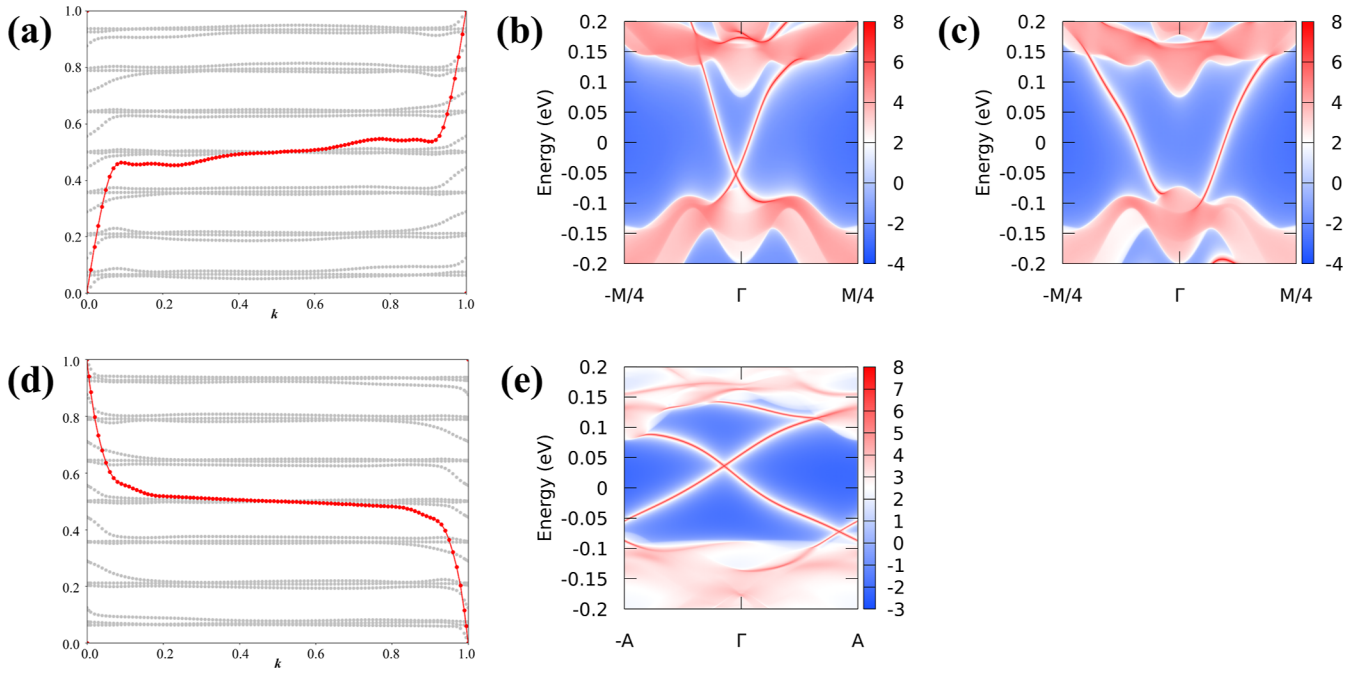

Figure 3. MCNs and surface LDOS of $MnBi_4Te_7$ in the FMx configuration. (a) WCC of the $m_x = +i$ subspace, (b) (001) surface LDOS on QL termination, (c) (001) surface LDOS on SL termination, (d) WCC of the $m_x = -i$ subspace, and (e) (010) surface LDOS.

center (WCC) to further confirm this result. As shown in Figure 1c, the Wilson loop also manifests that $\mathbb{Z}_2 = 1$ consistently as the blue reference line, which tracks the center of the largest WCC gap, crosses the WCCs odd times.[53−55] As the parity symmetry $\hat{P}$ exists, we can also diagnose the band topology by the $\mathbb{Z}_4$ topological invariant as follows

$$\mathbb{Z}_4 = \sum_{\alpha=1}^{8} \sum_{n=1}^{n_{occ}} \frac{1 + \xi_n(\Lambda_\alpha)}{2} \bmod 4 \tag{6}$$

where Λ_α represents the eight inversion invariant k points in the Brillouin zone, n runs over all the occupied bands, and $\xi_n(\Lambda_\alpha)$ is the parity eigenvalue of the nth band at Λ_α.[56,57] It is well-known that $\mathbb{Z}_4 = 1$ or 3 indicates a topological semimetal phase and $\mathbb{Z}_4 = 2$ indicates an AXI phase, while $\mathbb{Z}_4 = 0$ suggests a topological trivial phase. Employing eq 6, $\mathbb{Z}_4 = 2$ is obtained regardless of whether in the A-AFMx or FMx configuration, implying that $MnBi_4Te_7$ is an AXI in these states. As shown in Figure 1d, such nontrivial band topology originates from the inverted band gap between the Bi p and Te p orbitals at the Γ point, which is induced by the strong spin−orbit coupling (SOC) effect.

Then, we move onto exploring the possible TCI phase since the mirror symmetry $\hat{M}_x$ survived if the spins align along the x orientation. On the $k_x = 0$ plane, the reciprocal wave vectors are invariant under mirror operation $\hat{M}_x$, and the energy eigenstates are also mirror eigenstates, as follows

$$\hat{M}_x|n, k\rangle = m_x|n, k\rangle \tag{7}$$

where m_x is the mirror eigenvalue that can be $+i$ or $-i$ under the double group description. At this point, the mirror eigenstates can be divided into the $+i$ and $-i$ subspaces. Therefore, the mirror Chern number (MCN) can be calculated as

$$C_M = \frac{C_{+i} - C_{-i}}{2} \tag{8}$$

in which C_{+i} and C_{-i} are the Chern numbers defined in these two subspaces, respectively.

We obtain the MCN $C_M = 1$ based on eqs 7 and 8 via the topological quantum chemistry (TQC) and symmetry indicator (SI) method.[58−61] This indicates a mirror-symmetry-protected TCI phase. We also calculated the flow of WCC to obtain the MCN. As shown in Figure 2a,d, the Wilson loop suggests $C_{\pm i} = \pm 1$. To explore the topological surface states, we employed the iterative Green function method to calculate the local density of states (LDOS) confined to a specific surface based on the Wannier Hamiltonian. As shown in Figure 2b,c, the gapless surface states along the $k_x = 0$ path on the (001) slab emerge in the bulk band gap on the QL termination but are buried into the valence bands on the SL termination. These metallic surface states are purely protected by the mirror symmetry as the $\hat{T}\tau_{1/2}$ symmetry is broken on the (001) surface. As a result, the degenerate point shifts away from the Γ point. However, as shown in Figure 2e, the massless Dirac Fermion states emerge on the (010) surface since $\hat{T}\tau_{1/2}$ is preserved. These topological quantum states may be realized experimentally by a very weak external magnetic field as the magnetic anisotropic energy (MAE) is typically far less than the exchange energy, even by several orders of magnitude. Within our calculations, the MAE is 0.218 meV/Mn, which is obtained by calculating the energy difference between the FMx and FMz states. The energy of the A-AFM state is 1.63 meV/Mn lower than that of the FM state. We also calculate the intralayer magnetic coupling with a $2 \times 1 \times 1$ supercell. The energy of the in-plane FM state is 6.742 meV/Mn lower than that of the AFM state. This suggests that the intralayer FM coupling is stable. As for the $MnSb_4Te_7$, the estimated MAE, interlayer magnetic coupling strength, and intralayer magnetic

https://doi.org/10.1021/acs.jpcc.4c05870
J. Phys. Chem. C 2024, 128, 20451−20458

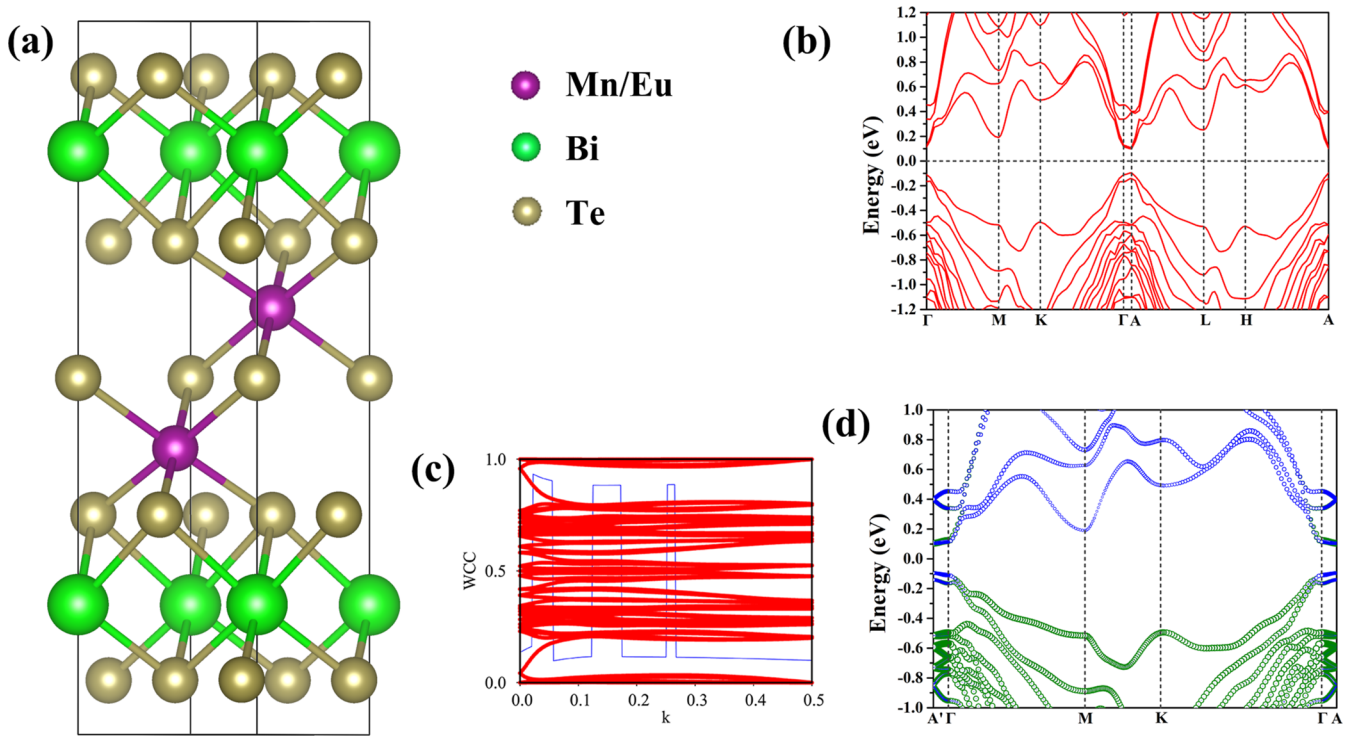

Figure 4. Crystal and electronic structures of $Mn_2Bi_2Te_5$. (a) Crystal structure of $Mn_2Bi_2Te_5$ or $Eu_2Bi_2Te_5$, (b) bulk band structure of $Mn_2Bi_2Te_5$ in the FMx_w-AFM$_b$ configuration, (c) WCC of $Mn_2Bi_2Te_5$ in the FMx_w-AFM$_b$ configuration, and (d) projected inverted band of $Mn_2Bi_2Te_5$ in the FMx_w-AFM$_b$ configuration, in which the blue bubbles represent the Bi p orbital projection and the olive bubbles represent the Te p orbital projection.

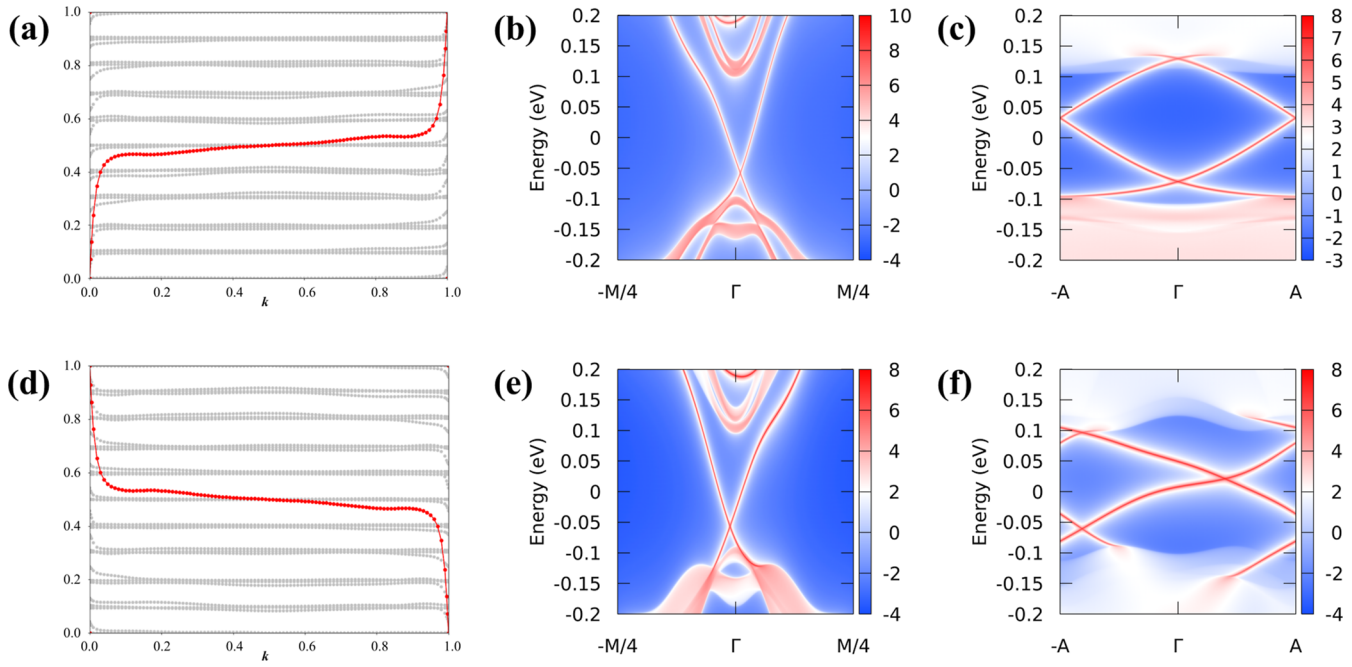

Figure 5. MCNs and surface LDOS of $Mn_2Bi_2Te_5$. (a) WCC of the $m_x = +i$ subspace in the FMx_w-AFM$_b$ configuration, (b) (001) surface LDOS in the FMx_w-AFM$_b$ configuration, (c) (010) surface LDOS in the FMx_w-AFM$_b$ configuration, (d) WCC of the $m_x = -i$ subspace in the FMx_w-AFM$_b$ configuration, (e) (001) surface LDOS in the FMx configuration, and (f) (010) surface LDOS in the FMx configuration.

coupling strength are 0.0795, 0.38, and 8.115 meV/Mn, respectively.

When turned to the FMx configuration, the mirror symmetry $\widehat{M}_x$ is still survived, but the $\widehat{T}\tau_{1/2}$ is broken. The bulk band structure and projected inverted band gap are similar to those in the A-AFMx configuration and can be found in Section II of Supporting Information. The Kramer degeneracy is removed in the FM state as the $\widehat{T}\tau_{1/2}$ symmetry is broken. However, since the Bi p and Te p bands are inverted near the Γ point, the topologically nontrivial nature is still

https://doi.org/10.1021/acs.jpcc.4c05870
J. Phys. Chem. C 2024, 128, 20451−20458

preserved. Here, we obtained $\mathbb{Z}_4 = 2$ in the FMx state according to eq 6. As shown in Figure 3a,d, we obtain $C_{\pm i} = \pm 1$ and $C_M = 1$ according to eq 8. Thus, $MnBi_4Te_7$ is a TCI in the FMx state. As shown in Figure 3b,c, the gapless topological surface states are analogous to those in the A-AFMx configuration on the (001) surface. However, as shown in Figure 3e, it is worth noting that on the (010) surface, the degenerate point of the topological surface states is away from the Γ point since $\widehat{T}\tau_{1/2}$ is broken and the band topology is purely protected by the $\widehat{M}_x$ symmetry. In our calculations, the electronic structure and band topology of $MnSb_4Te_7$ are very similar to those of $MnBi_4Te_7$ regardless of whether in the A-AFMx or FMx configuration; thus, we have included these details in Section III of the Supporting Information.

As for $Mn_2Bi_2Te_5$, things are far more complicated. The crystal structure of $Mn_2Bi_2Te_5$ and $Eu_2Bi_2Te_5$ is shown in Figure 4a. These compounds are built with hexagonal nonuple layers (NLs).[62,63] Unlike $Mn(Bi, Sb)_4Te_7$, the theoretically predicted magnetic ground state and band topology of $Mn_2Bi_2Te_5$ are very sensible to the Hubbard U values of Mn 3d orbitals, which have been carefully tested by Eremeev et al.[64] In Eremeev's work, within a NL block, $Mn_2Bi_2Te_5$ favors AFM coupling (AFM_w) when $U \leq 3$ eV but FM coupling (FM_w) when $U \geq 4$ eV. However, the interblock coupling is AFM (AFM_b) regardless of whether the U value is 3 or 5 eV. Furthermore, in the FM configuration, $Mn_2Bi_2Te_5$ is an AXI calculated with the final $U = 5.34$ eV in Eremeev's work. But we note that FM Weyl semimetal phases are reported with $U = 3$ eV.[65] Here, we adopted $U = 5.34$ eV, the same as Eremeev's work, and that we used for $Mn(Bi, Sb)_4Te_7$. In FMx_w-AFM_b and FMx states, the magnetic space groups of $Mn_2Bi_2Te_5$ are the same as that of $Mn(Bi, Sb)_4Te_7$, namely, C_c2/m and $C2/m$, respectively. The band structure and inverted band gap of $Mn_2Bi_2Te_5$ in the FMx_w-AFM_b configuration are shown in Figure 4b,d. The FMx band structure and inverted band gap can be found in Section IV of the Supporting Information. As shown in Figure 4c, the WCC suggests that $\mathbb{Z}_2 = 1$; thus, it is an AFM TI in the FMx_w-AFM_b configuration. Furthermore, $\mathbb{Z}_4 = 2$ is obtained via eq 6 in both FMx_w-AFM_b and FMx configurations, indicating the AXI phases.

Protected by the mirror symmetry $\widehat{M}_x$ and inverted bands, nontrivial MCNs $C_{\pm i} = \pm 1$ are obtained in FMx_w-AFM_b, as shown in Figure 5a,d. The MCNs in the FMx configuration can be found in Section IV of the Supporting Information. As a result of $C_M = 1$ and $\mathbb{Z}_2 = 1$, gapless topological surface states emerge on the (001) and (010) surfaces in the FMx_w-AFM_b configuration, as shown in Figure 5b,c. As shown in Figure 5e,f, such mirror-symmetry-protected gapless surface states also emerge on these slabs since the $\widehat{M}_x$ symmetry is maintained in the FMx configuration. Therefore, we predict that $Mn_2Bi_2Te_5$ is also a possible mirror-symmetry-protected TCI candidate in FMx_w-AFM_b and FMx configurations based on our calculations.

Last but not least, we also predicted that $Eu_2Bi_2Te_5$ has a similar TCI phase in its FMx configuration. The $C_{\pm i} = \pm 1$ MCNs, band structure, and gapless topological surface states can be found in Section V of Supporting Information. We discover that the magnetic ground state of $Eu_2Bi_2Te_5$ is simply AFM between Mn planes along the z axis, in line with the work of Zhang et al.[66] Hence, it cannot be a TCI in the AFM state since the mirror symmetry is broken. However, we find that the magnetic easy axis is along the in-plane direction, which is also consistent with the work of Wang et al. This implies that the FMx configuration can be more easily realized since there is no MAE barrier. To further confirm this result, we employ the more accurate r^{2}SCAN-D4 + U method.[67] We find that the predicted magnetic easy axis is unchanged under U values of 6, 7, and 8 eV for Eu 4f. The MAE value is so small, around 0.01 meV/Eu, which is similar to that reported by Wang et al. Therefore, $Eu_2Bi_2Te_5$ may be an excellent platform to realize an FM TCI phase.

SUMMARY

In conclusion, we predict that $MnBi_4Te_7$, $MnSb_4Te_7$, $Mn_2Bi_2Te_5$, and $Eu_2Bi_2Te_5$ are magnetic TCI candidates when spins align along the x direction. Mirror-symmetry-protected gapless topological surface states emerge on the (001) and (010) surfaces. Since the (001) surface is the vdW termination of these materials, it is more likely to be experimentally observed by ARPES measurements. Meanwhile, the magnetic easy axis of $Eu_2Bi_2Te_5$ is found to be the in-plane orientation in our calculations. Our work provides more opportunities for the study of magnetic topological physics and magnetically controllable topological quantum phase transitions.

ASSOCIATED CONTENT

Data Availability Statement

The data and input files for DFT calculations that support the findings of this study are available upon reasonable request from the authors.

Supporting Information

The Supporting Information is available free of charge at https://pubs.acs.org/doi/10.1021/acs.jpcc.4c05870.

Crystal structures, band structure of $MnBi_4Te_7$ in the FMx configuration, TCI phases of $MnSb_4Te_7$, band structure and MCNs of $Mn_2Bi_2Te_5$ in the FMx configuration, TCI phase of $Eu_2Bi_2Te_5$, and band structures without SOC (PDF)

AUTHOR INFORMATION

Corresponding Author

Yu-Jun Zhao − *Department of Physics, South China University of Technology, Guangzhou 510640, People's Republic of China;* orcid.org/0000-0002-6923-1099; Email: zhaoyj@scut.edu.cn

Authors

Jia-Yi Lin − *Department of Physics, South China University of Technology, Guangzhou 510640, People's Republic of China*

Zhipeng Cao − *Key Laboratory of Quantum Materials and Devices of Ministry of Education, School of Physics, Southeast University, Nanjing 211189, China*

Zhong-Jia Chen − *Songshan Lake Materials Laboratory, Dongguan, Guangdong 523808, China;* orcid.org/0000-0003-0345-7447

Wenxin He − *Department of Physics, Southern University of Science and Technology, Shenzhen 518055, China*

Jiarui Zeng − *School of Physics and Optoelectronic Engineering, Hainan University, Haikou 570228, China*

Xiao-Bao Yang − *Department of Physics, South China University of Technology, Guangzhou 510640, People's Republic of China;* orcid.org/0000-0001-8851-1988

https://doi.org/10.1021/acs.jpcc.4c05870
J. Phys. Chem. C 2024, 128, 20451−20458

Yichen Hua − *Department of Physics, Southern University of Science and Technology, Shenzhen 518055, China*
Ji-Hai Liao − *Department of Physics, South China University of Technology, Guangzhou 510640, People's Republic of China*

Complete contact information is available at: https://pubs.acs.org/10.1021/acs.jpcc.4c05870

Author Contributions

[#]J.-Y.L. and Z.C. contributed equally to this work.

Notes

The authors declare no competing financial interest.

■ ACKNOWLEDGMENTS

Jia-Yi Lin greatly thanks Prof. Eremeev (eremeev@ispms.tsc.ru) for the structural information on $Mn_2Bi_2Te_5$. This work is financially supported by the National Natural Science Foundation of China (Grant No. 12074126) and the Guangdong Basic and Applied Basic Research Foundation (No. 2023A1515012289).

■ REFERENCES

(1) Moore, J. E. The Birth of Topological Insulators. *Nature* **2010**, *464*, 194−198.
(2) Bampoulis, P.; Castenmiller, C.; Klaassen, D. J.; van Mil, J.; Liu, Y.; Liu, C.-C.; Yao, Y.; Ezawa, M.; Rudenko, A. N.; Zandvliet, H. J. W. Quantum Spin Hall States and Topological Phase Transition in Germanene. *Phys. Rev. Lett.* **2023**, *130*, 196401.
(3) Chiu, C.-K.; Teo, J. C. Y.; Schnyder, A. P.; Ryu, S. Classification of Topological Quantum Matter with Symmetries. *Rev. Mod. Phys.* **2016**, *88*, 035005.
(4) Chang, C.-Z.; Zhang, J.; Feng, X.; Shen, J.; Zhang, Z.; Guo, M.; Li, K.; Ou, Y.; Wei, P.; Wang, L.-L.; et al. Experimental Observation of the Quantum Anomalous Hall Effect in a Magnetic Topological Insulator. *Science* **2013**, *340*, 167−170.
(5) Lv, B. Q.; Qian, T.; Ding, H. Experimental Perspective on Three-Dimensional Topological Semimetals. *Rev. Mod. Phys.* **2021**, *93*, 025002.
(6) Sato, M.; Ando, Y. Topological Superconductors: A Review. *Rep. Prog. Phys.* **2017**, *80*, 076501.
(7) Zhang, T.; Jiang, Y.; Song, Z.; Huang, H.; He, Y.; Fang, Z.; Weng, H.; Fang, C. Catalogue of Topological Electronic Materials. *Nature* **2019**, *566*, 475−479.
(8) Tang, F.; Po, H. C.; Vishwanath, A.; Wan, X. Comprehensive Search for Topological Materials Using Symmetry Indicators. *Nature* **2019**, *566*, 486−489.
(9) Vergniory, M. G.; Elcoro, L.; Felser, C.; Regnault, N.; Bernevig, B. A.; Wang, Z. A Complete Catalogue of High-quality Topological Materials. *Nature* **2019**, *566*, 480−485.
(10) Vergniory, M. G.; Wieder, B. J.; Elcoro, L.; Parkin, S. S. P.; Felser, C.; Bernevig, B. A.; Regnault, N. All Topological Bands of All Nonmagnetic Stoichiometric Materials. *Science* **2022**, *376*, No. eabg9094.
(11) Xu, Y.; Vergniory, M. G.; Ma, D.-S.; Mañes, J. L.; Song, Z.-D.; Bernevig, B. A.; Regnault, N.; Elcoro, L. Catalog of Topological Phonon Materials. *Science* **2024**, *384*, No. eadf8458.
(12) Mong, R. S. K.; Essin, A. M.; Moore, J. E. Antiferromagnetic Topological Insulators. *Phys. Rev. B* **2010**, *81*, 245209.
(13) Otrokov, M. M.; Klimovskikh, I. I.; Bentmann, H.; Estyunin, D.; Zeugner, A.; Aliev, Z. S.; Gaß, S.; Wolter, A. U. B.; Koroleva, A. V.; Shikin, A. M.; et al. Prediction and Observation of an Antiferromagnetic Topological Insulator. *Nature* **2019**, *576*, 416−422.
(14) Zhang, D.; Shi, M.; Zhu, T.; Xing, D.; Zhang, H.; Wang, J. Topological Axion States in the Magnetic Insulator $MnBi_2Te_4$ with the Quantized Magnetoelectric Effect. *Phys. Rev. Lett.* **2019**, *122*, 206401.
(15) Yang, S.; Xu, X.; Zhu, Y.; Niu, R.; Xu, C.; Peng, Y.; Cheng, X.; Jia, X.; Huang, Y.; Xu, X.; et al. Odd-Even Layer-Number Effect and Layer-Dependent Magnetic Phase Diagrams in $MnBi_2Te_4$. *Phys. Rev. X* **2021**, *11*, 011003.
(16) Deng, Y.; Yu, Y.; Shi, M. Z.; Guo, Z.; Xu, Z.; Wang, J.; Chen, X. H.; Zhang, Y. Quantum Anomalous Hall Effect in Intrinsic Magnetic Topological Insulator $MnBi_2Te_4$. *Science* **2020**, *367*, 895−900.
(17) Zang, Z.; Zhu, Y.; Xi, M.; Tian, S.; Wang, T.; Gu, P.; Peng, Y.; Yang, S.; Xu, X.; Li, Y.; et al. Layer-Number-Dependent Antiferromagnetic and Ferromagnetic Behavior in $MnSb_2Te_4$. *Phys. Rev. Lett.* **2022**, *128*, 017201.
(18) Eremeev, S. V.; Rusinov, I. P.; Koroteev, Y. M.; Vyazovskaya, A. Y.; Hoffmann, M.; Echenique, P. M.; Ernst, A.; Otrokov, M. M.; Chulkov, E. V. Topological Magnetic Materials of the $(MnSb_2Te_4)\cdot(Sb_2Te_3)_n$ van der Waals Compounds Family. *J. Phys. Chem. Lett.* **2021**, *12*, 4268−4277.
(19) Zhu, T.; Bishop, A. J.; Zhou, T.; Zhu, M.; O'Hara, D. J.; Baker, A. A.; Cheng, S.; Walko, R. C.; Repicky, J. J.; Liu, T.; et al. Synthesis, Magnetic Properties, and Electronic Structure of Magnetic Topological Insulator $MnBi_2Se_4$. *Nano Lett.* **2021**, *21*, 5083−5090.
(20) Zhan, F.; Qin, Z.; Xu, D.-H.; Zhou, X.; Ma, D.-S.; Wang, R. Design of Antiferromagnetic Second-Order Band Topology with Rotation Topological Invariants in Two Dimensions. *Nano Lett.* **2024**, *24*, 7741−7747.
(21) Yuan, W.; Yan, Z.-J.; Yi, H.; Wang, Z.; Paolini, S.; Zhao, Y.-F.; Zhou, L.; Wang, A. G.; Wang, K.; Prokscha, T.; et al. Coexistence of Superconductivity and Antiferromagnetism in Topological Magnet $MnBi_2Te_4$ Films. *Nano Lett.* **2024**, *24*, 7962−7971.
(22) Kaplan, D.; Holder, T.; Yan, B. Unification of Nonlinear Anomalous Hall Effect and Nonreciprocal Magnetoresistance in Metals by the Quantum Geometry. *Phys. Rev. Lett.* **2024**, *132*, 026301.
(23) Li, Y.; Wang, Y.; Lian, Z.; Li, H.; Gao, Z.; Xu, L.; Wang, H.; Lu, R.; Li, L.; Feng, Y.; et al. Fabrication-Induced Even-Odd Discrepancy of Magnetotransport in Few-Layer $MnBi_2Te_4$. *Nat. Commun.* **2024**, *15*, 3399.
(24) Chong, S. K.; Cheng, Y.; Man, H.; Lee, S. H.; Wang, Y.; Dai, B.; Tanabe, M.; Yang, T.-H.; Mao, Z.; Moler, K. A.; et al. Intrinsic Exchange Biased Anomalous Hall Effect in an Uncompensated Antiferromagnet $MnBi_2Te_4$. *Nat. Commun.* **2024**, *15*, 2881.
(25) Rodriguez-Vega, M.; Lin, Z.-X.; Leonardo, A.; Ernst, A.; Vergniory, M. G.; Fiete, G. A. Light-Driven Topological and Magnetic Phase Transitions in Thin Layer Antiferromagnets. *J. Phys. Chem. Lett.* **2022**, *13*, 4152−4158.
(26) Ahn, J.; Kang, S.-H.; Yoon, M.; Ganesh, P.; Krogel, J. T. Stacking Faults and Topological Properties in $MnBi_2Te_4$: Reconciling Gapped and Gapless States. *J. Phys. Chem. Lett.* **2023**, *14*, 9052−9059.
(27) Xi, M.; Chen, F.; Gong, C.; Tian, S.; Yin, Q.; Qian, T.; Lei, H. Relationship between Antisite Defects, Magnetism, and Band Topology in $MnSb_2Te_4$ Crystals with $T_C \approx 40$ K. *J. Phys. Chem. Lett.* **2022**, *13*, 10897−10904.
(28) Fu, L. Topological Crystalline Insulators. *Phys. Rev. Lett.* **2011**, *106*, 106802.
(29) Hsieh, T. H.; Lin, H.; Liu, J.; Duan, W.; Bansil, A.; Fu, L. Topological Crystalline Insulators in the SnTe Material Class. *Nat. Commun.* **2012**, *3*, 982−987.
(30) Li, J.; Wang, C.; Zhang, Z.; Gu, B.-L.; Duan, W.; Xu, Y. Magnetically Controllable Topological Quantum Phase Transitions in the Antiferromagnetic Topological Insulator $MnBi_2Te_4$. *Phys. Rev. B* **2019**, *100*, 121103.
(31) Lin, J.-Y.; Chen, Z.-J.; Cao, Z.; Zeng, J.; Yang, X.-B.; Yao, Y.; Zhao, Y.-J. Multiple Magnetic Topological Phases in the van der Waals Crystal $Mn(Bi,Sb)_4Se_7$. *J. Phys. Chem. Lett.* **2023**, *14*, 3913−3919.
(32) Kresse, G.; Furthmüller, J. Efficiency of ab-initio Total Energy Calculations for Metals and Semiconductors Using a Plane-Wave Basis Set. *Comput. Mater. Sci.* **1996**, *6*, 15−50.
(33) Kresse, G.; Hafner, J. *Ab initio* Molecular Dynamics for Open-Shell Transition Metals. *Phys. Rev. B* **1993**, *48*, 13115−13118.

(34) Kresse, G.; Hafner, J. *Ab initio* Molecular Dynamics for Liquid Metals. *Phys. Rev. B* **1993**, *47*, 558−561.
(35) Perdew, J. P.; Burke, K.; Ernzerhof, M. Generalized Gradient Approximation Made Simple. *Phys. Rev. Lett.* **1996**, *77*, 3865−3868.
(36) Kresse, G.; Joubert, D. From Ultrasoft Pseudopotentials to the Projector Augmented-Wave Method. *Phys. Rev. B* **1999**, *59*, 1758−1775.
(37) Blöchl, P. E. Projector Augmented-Wave Method. *Phys. Rev. B* **1994**, *50*, 17953−17979.
(38) Kresse, G.; Furthmüller, J. Efficient Iterative Schemes for *ab initio* Total-Energy Calculations Using a Plane-Wave Basis Set. *Phys. Rev. B* **1996**, *54*, 11169−11186.
(39) Anisimov, V. I.; Zaanen, J.; Andersen, O. K. Band Theory and Mott Insulators: Hubbard *U* Instead of Stoner *I*. *Phys. Rev. B* **1991**, *44*, 943−954.
(40) Dudarev, S. L.; Botton, G. A.; Savrasov, S. Y.; Humphreys, C. J.; Sutton, A. P. Electron-Energy-Loss Spectra and the Structural Stability of Nickel Oxide: An LSDA+U Study. *Phys. Rev. B* **1998**, *57*, 1505−1509.
(41) Caldeweyher, E.; Mewes, J.-M.; Ehlert, S.; Grimme, S. Extension and Evaluation of the D4 London-Dispersion Model for Periodic Systems. *Phys. Chem. Chem. Phys.* **2020**, *22*, 8499−8512.
(42) Gao, J.; Wu, Q.; Persson, C.; Wang, Z. Irvsp: to Obtain Irreducible Representations of Electronic States in the VASP. *Comput. Phys. Commun.* **2021**, *261*, 107760.
(43) Elcoro, L.; Wieder, B. J.; Song, Z.; Xu, Y.; Bradlyn, B.; Bernevig, B. A. Magnetic Topological Quantum Chemistry. *Nat. Commun.* **2021**, *12*, 5965.
(44) Pizzi, G.; Vitale, V.; Arita, R.; Blügel, S.; Freimuth, F.; Géranton, G.; Gibertini, M.; Gresch, D.; Johnson, C.; Koretsune, T.; et al. Wannier90 as a Community Code: New Features and Applications. *J. Phys.: Condens. Matter* **2020**, *32*, 165902.
(45) Marzari, N.; Vanderbilt, D. Maximally Localized Generalized Wannier Functions for Composite Energy Bands. *Phys. Rev. B* **1997**, *56*, 12847−12865.
(46) Souza, I.; Marzari, N.; Vanderbilt, D. Maximally Localized Wannier Functions for Entangled Energy Bands. *Phys. Rev. B* **2001**, *65*, 035109.
(47) Wu, Q.; Zhang, S.; Song, H.-F.; Troyer, M.; Soluyanov, A. A. WannierTools: An Open-Source Software Package for Novel Topological Materials. *Comput. Phys. Commun.* **2018**, *224*, 405−416.
(48) Hu, C.; Gordon, K. N.; Liu, P.; Liu, J.; Zhou, X.; Hao, P.; Narayan, D.; Emmanouilidou, E.; Sun, H.; Liu, Y.; et al. A van der Waals Antiferromagnetic Topological Insulator with Weak Interlayer Magnetic Coupling. *Nat. Commun.* **2020**, *11*, 97−98.
(49) Huan, S.; Zhang, S.; Jiang, Z.; Su, H.; Wang, H.; Zhang, X.; Yang, Y.; Liu, Z.; Wang, X.; Yu, N.; et al. Multiple Magnetic Topological Phases in Bulk van der Waals Crystal $MnSb_4Te_7$. *Phys. Rev. Lett.* **2021**, *126*, 246601.
(50) Caldeweyher, E.; Ehlert, S.; Hansen, A.; Neugebauer, H.; Spicher, S.; Bannwarth, C.; Grimme, S. A Generally Applicable Atomic-Charge Dependent London Dispersion Correction. *J. Chem. Phys.* **2019**, *150*, 154122.
(51) Zhang, H.; Liu, C.-X.; Qi, X.-L.; Dai, X.; Fang, Z.; Zhang, S.-C. Topological Insulators in Bi_2Se_3, Bi_2Te_3 and Sb_2Te_3 with a Single Dirac Cone on the Surface. *Nat. Phys.* **2009**, *5*, 438−442.
(52) Fang, C.; Gilbert, M. J.; Bernevig, B. A. Topological Insulators with Commensurate Antiferromagnetism. *Phys. Rev. B* **2013**, *88*, 085406.
(53) Yu, R.; Qi, X. L.; Bernevig, A.; Fang, Z.; Dai, X. Equivalent Expression of Z_2 Topological Invariant for Band Insulators Using the non-Abelian Berry Connection. *Phys. Rev. B* **2011**, *84*, 075119.
(54) Soluyanov, A. A.; Vanderbilt, D. Wannier Representation of Z_2 Topological Insulators. *Phys. Rev. B* **2011**, *83*, 035108.
(55) Soluyanov, A. A.; Vanderbilt, D. Computing Topological Invariants without Inversion Symmetry. *Phys. Rev. B* **2011**, *83*, 235401.
(56) Xu, Y.; Song, Z.; Wang, Z.; Weng, H.; Dai, X. Higher-Order Topology of the Axion Insulator $EuIn_2As_2$. *Phys. Rev. Lett.* **2019**, *122*, 256402.
(57) Yue, C.; Xu, Y.; Song, Z.; Weng, H.; Lu, Y.-M.; Fang, C.; Dai, X. Symmetry-Enforced Chiral Hinge States and Surface Quantum Anomalous Hall Effect in the Magnetic Axion Insulator $Bi_{2-x}Sm_xSe_3$. *Nat. Phys.* **2019**, *15*, 577−581.
(58) Bradlyn, B.; Elcoro, L.; Cano, J.; Vergniory, M. G.; Wang, Z.; Felser, C.; Aroyo, M. I.; Bernevig, B. A. Topological Quantum Chemistry. *Nature* **2017**, *547*, 298−305.
(59) Gao, J.; Guo, Z.; Weng, H.; Wang, Z. Magnetic Band Representations, Fu-Kane-Like Symmetry Indicators, and Magnetic Topological Materials. *Phys. Rev. B* **2022**, *106*, 035150.
(60) Peng, B.; Jiang, Y.; Fang, Z.; Weng, H.; Fang, C. Topological Classification and Diagnosis in Magnetically Ordered Electronic Materials. *Phys. Rev. B* **2022**, *105*, 235138.
(61) Xu, Y.; Elcoro, L.; Song, Z.-D.; Wieder, B. J.; Vergniory, M. G.; Regnault, N.; Chen, Y.; Felser, C.; Bernevig, B. A. High-Throughput Calculations of Magnetic Topological Materials. *Nature* **2020**, *586*, 702−707.
(62) Cao, L.; Han, S.; Lv, Y.-Y.; Wang, D.; Luo, Y.-C.; Zhang, Y.-Y.; Yao, S.-H.; Zhou, J.; Chen, Y. B.; Zhang, H.; et al. Growth and Characterization of the Dynamical Axion Insulator Candidate $Mn_2Bi_2Te_5$ with Intrinsic Antiferromagnetism. *Phys. Rev. B* **2021**, *104*, 054421.
(63) Wang, M.; Liu, H.; Xie, X. C. New Type of Anticommutative Dynamical Magnetoelectric Response. *Phys. Rev. Lett.* **2022**, *128*, 236601.
(64) Eremeev, S. V.; Otrokov, M. M.; Ernst, A.; Chulkov, E. V. Magnetic Ordering and Topology in $Mn_2Bi_2Te_5$ and $Mn_2Sb_2Te_5$ van der Waals Materials. *Phys. Rev. B* **2022**, *105*, 195105.
(65) Li, Y.; Jiang, Y.; Zhang, J.; Liu, Z.; Yang, Z.; Wang, J. Intrinsic Topological Phases in $Mn_2Bi_2Te_5$ Tuned by the Layer Magnetization. *Phys. Rev. B* **2020**, *102*, 121107.
(66) Zhang, J.; Wang, D.; Shi, M.; Zhu, T.; Zhang, H.; Wang, J. Large Dynamical Axion Field in Topological Antiferromagnetic Insulator $Mn_2Bi_2Te_5$. *Chin. Phys. Lett.* **2020**, *37*, 077304.
(67) Furness, J. W.; Kaplan, A. D.; Ning, J.; Perdew, J. P.; Sun, J. Accurate and Numerically Efficient r^2 SCAN Meta-Generalized Gradient Approximation. *J. Phys. Chem. Lett.* **2020**, *11*, 8208−8215.

https://doi.org/10.1021/acs.jpcc.4c05870
J. Phys. Chem. C 2024, 128, 20451−20458